axioms

MDPI

Article

Topological Properties of the Intersection Curves Between a Torus and Families of Parabolic or Elliptical Cylinders

Ana Breda *,†, Alexandre Trocado † and José Dos Santos †

Center for Research & Development in Mathematics and Applications (CIDMA), Universidade de Aveiro, 3810-193 Aveiro, Portugal; mail@alexandretrocado.com (A.T.); dossantos@uc.pt (J.D.S.)

* Correspondence: ambreda@ua.pt

† These authors contributed equally to this work.

Abstract: This paper reports the research work carried out with the goal of geometrically and algebraically describing, as well as topologically classifying, the curves resulting from the intersection of a torus with families of parabolic and elliptical cylinders within a purely Euclidean framework. The parabolic cylinders under analysis have generatrices parallel to the axis of the torus, whereas the elliptical cylinders, centered at the same point as the torus, have axes either aligned with or orthogonal to the torus's axis. For the topological classification of these intersection curves, we consider their number of connected components and self-intersection points. GeoGebra, which was used to create the 3D visual geometric representations of the intersection curves, and Maple, which was used to perform the essential symbolic algebraic calculations, were critical computational tools in the development of this work. Theoretical and computational approaches are interwoven throughout this study, with the computational work serving as the foundation for exploration and providing insights that contributed to the theoretical validation of the results revealed through GeoGebra simulations.

Keywords: GeoGebra; toric sections; quadrics; surface/surface intersection

MSC: 51N20; 13P15; 14Q10; 65D18

check for updates

Citation: Breda, A.; Trocado, A.; Dos Santos, J. Topological Properties of the Intersection Curves Between a Torus and Families of Parabolic or Elliptical Cylinders. *Axioms* **2024**, *13*, 852. https://doi.org/10.3390/axioms13120852

Academic Editor: Luca Vitagliano

Received: 20 October 2024
Revised: 21 November 2024
Accepted: 27 November 2024
Published: 3 December 2024

Copyright: © 2024 by the authors. Licensee MDPI, Basel, Switzerland. This article is an open access article distributed under the terms and conditions of the Creative Commons Attribution (CC BY) license (https://creativecommons.org/licenses/by/4.0/).

1. Introduction

The surface intersection problem has been of great interest due to its wide-ranging applications in fields such as mathematics, physics, computer graphics, and computer-aided geometric design. Indeed, this area has captured the attention of researchers for decades due to its mathematical complexity and practical importance. As discussed by Tu et al. [1], there is a vast literature on the intersection of two quadrics, including classical results in algebraic geometry and modern results in computer-aided geometric design. The classical perspective develops within the framework of complex projective space, meaning that the results cannot be applied directly. The potential to efficiently calculate intersection curves between surfaces is important for CAD systems prioritizing design accuracy and precision, such as those used in mechanical components, architectural designs, aerospace structures, solid modeling, and robotics. For instance, Hanna emphasized the importance of accurately representing the intersection curve of two parametric surfaces [2], stating that "One must distinguish between finding the shape of the intersection curve, which might only be useful for display, and finding an accurate mathematical representation of the curve". Such distinctions are critical for ensuring both practical usability and scientific rigor. The study of the intersection curves of a torus with a cylinder is also essential for the physical description and geometric modeling of toroidal sections of magnetic confinement devices, such as tokamaks, which have a toroidal shape [3].

Among the significant contributions to the study of torus intersections with other natural quadrics (spheres, right circular cylinders, and cones) [4,5] are those of Ku-Jin Kim [6], who developed a system to compute all circles within the intersection curves

of two tori, and the Liu et al. algorithm [7] for determining the intersection curve, also between two tori. These foundational works laid the groundwork for tackling more complex intersection problems.

Research into the detection and classification of intersection curves between a torus and a natural quadric, incorporating geometric, algebraic, and topological approaches [8], is still in its early stages. Recently, however, there has been a shift toward integrating these diverse methodologies to leverage their respective advantages while mitigating their disadvantages, as seen in [4,9,10], which presented exact, robust, and practical methods for computing an explicit representation of the intersection of two arbitrary quadrics.

In this context, one particularly effective approach is the application of the subresultant theorem for multivariate polynomials. This method, supported by computational tools such as GeoGebra, namely, version 5.2.817.0-d (6 December 2023) [11], and Maple (March 2024) [12], allows for precise geometric visualization and symbolic algebraic computation.

The research work reported here is a follow-up to the study in [13], which considered intersections between a torus and families of non-natural quadrics, where the topological classification of the intersection curves of a torus with an ellipsoid was presented. Building upon these findings, we detail the methodology and procedures used to analyze, from geometric, algebraic, and topological perspectives, the intersection of a torus with families of parabolic and elliptical cylinders within a purely Euclidean framework. Due to the complexity of the problem, our analysis focuses on families of parabolic cylinders, with generatrices parallel to the torus's axis, and families of elliptical cylinders, where the cylinder's axis is either coincident with or orthogonal to the torus's axis.

Our approach adopts the terminology and the subresultant method for multivariate polynomials described in [13] to develop an algorithm that effectively meets our objectives. We also use the 3D capabilities of GeoGebra to generate geometric representations of the intersection curves and Maple's algebraic and symbolic tools to carry out the necessary algebraic computations within the developed algorithm.

The surface intersection problem has broad applications. In particular, intersections between a torus and a cylinder are important tools for mathematical modeling. Contributions to this topic have been made by Kim and Liu concerning the computing of intersection curves between torus and natural quadrics. Recent work has combined geometric, algebraic, and topological methods. This study extends previous research on torus intersections with non-natural quadrics, focusing on parabolic and elliptical cylinders.

To guide the reader through this work, in the following sections, we proceed with the algebraic characterization of the surfaces under study in Section 2. In Section 3, we present the algorithm that will provide an accurate representation of the intersection curves of the surfaces to classify them topologically by considering two families of quadrics. In the first case, we consider a family of parabolic cylinders whose axes are parallel and concentric with those of the torus in Section 4. In the second case, we address the intersection with a family of parabolic cylinders whose plane of symmetry is perpendicular to the equatorial plane of the torus in Section 5. We conclude this work with some considerations for future work.

2. Algebraic Characterization of the Surfaces Under Study

Let us begin by algebraically describing the surfaces involved in this research study:

- The torus $\mathcal{T} \equiv \mathcal{T}_{(O,rM,rm)}$.
  Let $\mathcal{T}$ be a torus centered at the origin, $O = (0,0,0)$, of the Cartesian coordinate system, with its axis along the z-axis.
  Denoting the radius from the center of the hole to the center of the torus tube by rM and the radius of the tube by rm, where $rM > rm$, $\mathcal{T} \equiv T_{(O,rM,rm)}$, can be described by the algebraic equation

$$\mathcal{T}_{(O,rM,rm)} : (x^2 + y^2 + z^2 + rM^2 - rm^2)^2 - 4\,rM^2\,(x^2 + y^2) = 0. \quad (1)$$

- The family of elliptic cylinders, $(\mathcal{E}_{(a,b)})_{a,b\in\mathbb{R}^+}$, centered at $O = (0,0,0)$ with axes coincident to the torus's axis.
  The elements of the family $(\mathcal{E}_{(a,b)})_{a,b\in\mathbb{R}^+}$ can be described algebraically by the equation
  $$\mathcal{E}_{(a,b)} : \frac{x^2}{a^2} + \frac{y^2}{b^2} - 1 = 0, \tag{2}$$
  where a and b are two positive real numbers.
- The family of elliptic cylinders centered at $O = (0,0,0)$ with axes orthogonal to the torus's axis.
  Without loss of generality, we can limit the study to the family of elliptic cylinders, $(\mathcal{E}_{(b,c)})_{c,d\in\mathbb{R}^+}$, centered at $O = (0,0,0)$ and axis Ox. Accordingly, the elements of the family $(\mathcal{E}_{(b,c)})_{c,d\in\mathbb{R}^+}$ can be described algebraically by the equation
  $$\mathcal{E}_{(b,c)} : \frac{y^2}{b^2} + \frac{z^2}{c^2} - 1 = 0, \tag{3}$$
  where b and c are two positive real numbers.
- The family of parabolic cylinders with generatrices parallel to the axis of the torus $\mathcal{T}$.
  Considering the rotational symmetry of $\mathcal{T}$, we can limit our study, without loss of generality, to the family of parabolic cylinders $(\mathcal{P}_{a,b})_{a,b\in\mathbb{R}^+}$, whose elements can be algebraically described by the equation
  $$\mathcal{P}_{(a,b)} : \frac{x^2}{a^2} - \frac{y}{b} - 1 = 0, \tag{4}$$
  where a and b are two positive real numbers.

3. Algorithm

In this section, we briefly present the procedure (algorithm) used to determine the intersection curve between the torus T and the elements of the elliptical and parabolic cylinder families under consideration. Roughly speaking, it involves the geometric and topological properties of the intersection curve's projection onto a 2D plane, the analysis of its critical and singular points, and, based on this analysis, the reconstruction of the intersection curve in 3D space, ensuring accurate and algebraically correct computations at each step, as follows:

1. Compute the squarefree polynomial $\mathbf{S}_0(x,y)$ corresponding to the **resultant** of the two surface polynomial equations, in terms of z. This step allows the projection of the intersection curve onto the xOy-plane to be described.
2. Describe the admissible region $\mathcal{A}$, contained in the intersection of the projections of the two surfaces onto the xOy-plane. This region contains the cutcurve, part of the curve $\mathbf{S}_0$ that lies within $\mathcal{A}$.
3. Compute the critical points of the curve $\mathbf{S}_0(x,y) = 0$, which are determined by the roots of the **resultant** $\left(\mathbf{S}_0(x,y), \frac{\partial \mathbf{S}_0}{\partial y}(x,y); y\right)$, and detect its singular points by solving $\frac{\partial \mathbf{S}_0}{\partial y}(x,y) = 0$. This step is essential for the subsequent lifting step.
4. Compute the regular points of the curve $\mathbf{S}_0(x,y) = 0$ that lie on the critical lines. The lifting of these regular points is performed using the implicit torus or the corresponding quadric equation.
5. Compute the points of the cutcurve that lie in the silhouette curves (the outer boundary of the projected surfaces onto the xOy-plane). These points will never be lifted.
6. Use the previously computed information to determine the topology of the curve.
7. Compute the branches of the cutcurve inside the admissible region using closed formulae involving radicals.
8. Obtain the intersection curve of the two considered surfaces by lifting the branches of the cutcurve using parametric equations of the torus.
   For a more detailed explanation of this algorithm, see [9,13].

4. The Intersection Curves of the Torus $\mathcal{T}$ with the Cylinder Families $(\mathcal{E}_{a,b})_{a,b\in\mathbb{R}^+}$, $(\mathcal{E}_{c,d})_{c,d\in\mathbb{R}^+}$, and $(\mathcal{P}_{a,b})_{a,b\in\mathbb{R}^+}$

The study of the intersection curves resulting from the intersection of the torus with the previously specified families of cylinders is carried out separately for each of the families.

4.1. The Case $\mathcal{T}\cap(\mathcal{E}_{a,b})_{a,b\in\mathbb{R}^+}$

Following the procedure described in Section 3, we start by computing the projection of the intersection curve of $\mathcal{T}$ with the elliptic cylinder $\mathcal{E}_{(a,b)}$ onto the xOy-plane.

Consider

$$\mathcal{T}_{(O,rM,rm)} = z^4 + t_2 z^2 + t_0 \quad \text{and} \quad \mathcal{E}_{(a,b)} : \frac{x^2}{a^2} + \frac{y^2}{b^2} - 1,$$

where

$t_2 = 2rM^2 - 2rm^2 + 2x^2 + 2y^2$,

$t_0 = rM^4 - 2rM^2rm^2 - 2rM^2x^2 - 2rM^2y^2 + rm^4 - 2rm^2x^2 - 2rm^2y^2 + x^4 + 2x^2y^2 + y^4$,

and $q_0 = \frac{x^2}{a^2} + \frac{y^2}{b^2} - 1$.

$$\begin{vmatrix} 1 & 0 & t_2 & 0 & t_0 & 0 \\ 0 & 1 & 0 & t_2 & 0 & t_0 \\ 0 & 0 & q_0 & 0 & 0 & 0 \\ 0 & 0 & 0 & q_0 & 0 & 0 \\ 0 & 0 & 0 & 0 & q_0 & 0 \\ 0 & 0 & 0 & 0 & 0 & q_0 \end{vmatrix} = \left(\frac{x^2}{a^2} + \frac{y^2}{b^2} - 1\right)^4,$$

Thus, the resultant is represented by the squarefree polynomial

$$S_0 = a^2b^2 - y^2a^2 - x^2b^2.$$

Also, using Maple, S_0 is computed, as shown in Figure 1.

```
> with(LinearAlgebra):
> eT := collect((x^2+y^2+z^2+rM^2-rm^2)^2-4*rM^2*(x^2+y^2), z);
                  eT := z^4 + (2 rM^2 - 2 rm^2 + 2 x^2 + 2 y^2) z^2 + (rM^2 - rm^2 + x^2 + y^2)^2 - 4 rM^2 (x^2 + y^2)
> eC := (x/a)^2 + (y/b)^2-1;
                                        eC := x^2/a^2 + y^2/b^2 - 1
> resultant(eC, eT, z);
                                        (a^2 b^2 - a^2 y^2 - b^2 x^2)^4 / (a^8 b^8)
```

Figure 1. Maple computations.

The cutcurve is contained within the admissible region $\mathcal{A}$, which, in turn, is contained within the region

$$(rM - rm)^2 \le x^2 + y^2 \le (rM + rm)^2.$$

Using the geometric representation and CAS functionalities of GeoGebra, complemented by the symbolic computation power of Maple and applying the strategies described in [13], we can explore all possible configurations for the case under study by considering the viable variations of the parameters a and b. These configurations are detailed in Table 1.

Next, we present the results for all admissible variations of the parameters a and b. It is important to emphasize that the methodology used guarantees the mathematical validity of the stated conclusions. The geometric representations are corroborated by symbolic algebraic computations, and vice versa.

Table 1. Geometric representations and topological properties (number of connected components and self-intersection points) of $\mathcal{T} \cap \mathcal{E}_{(a,b)}$.

	$b < rM - rm$	$b = rM - rm$	$rM - rm < b < rm + rM$	$b = rm + rM$	$b > rm + rM$
$a < rM - rm$	$\emptyset$ (Figure 2a)	2 points (Figure 2b)	2 c.c. (Figure 2c)	2 c.c. 2 a.p. (Figure 2d)	4 c.c. (Figure 2e)
$a = rM - rm$	2 points (Figure 3a)	1 c.c. (Figure 3b)	1 c.c. 2 a.p. (Figure 3c)	1 c.c. 4 a.p. (Figure 3d)	2 c.c. 2 a.p. (Figure 3e)
$rM - rm < a < rm + rM$	2 c.c. (Figure 4a)	1 c.c. (Figure 4b)	2 c.c. (Figure 4c)	1 c.c. 2 a.p. (Figure 4d)	2 c.c. (Figure 4e)
$a = rm + rM$	2 c.c. 2 a.p. (Figure 5a)	1 c.c. 4 a.p. (Figure 5b)	1 c.c. 2 a.p. (Figure 5c)	1 c.c. (Figure 5d)	2 points (Figure 5e)
$a > rm + rM$	4 c.c. (Figure 6a)	2 c.c. (Figure 6b)	2 c.c. (Figure 6c)	2 points (Figure 6d)	$\emptyset$ (Figure 6e)

4.1.1. First, Assume That $a < rM - rm$

We consider the following cases:

- If $b < rM - rm$, the cylinder is inside the torus hole, and so the intersection of the two surfaces is the empty set (Figure 2a).
- If $b = rM - rm$, the cylinder touches the torus tangentially at the points $(0, \pm(rM - rm), 0)$ (Figure 2b). The intersection set is composed of these two isolated points.
- If $rM - rm < b < rM + rm$, the intersection curve has two connected components (Figure 2c).
- If $b = rM + rm$, the intersection curve has two connected components, each with a self-intersection at coordinates $(0, \pm(rM + rm), 0)$ (Figure 2d). In this case, the outer equatorial circle of the torus tangentially touches the cylinder at the specified points.
- If $b > rM + rm$, the intersection curve has four connected components (Figure 2e).

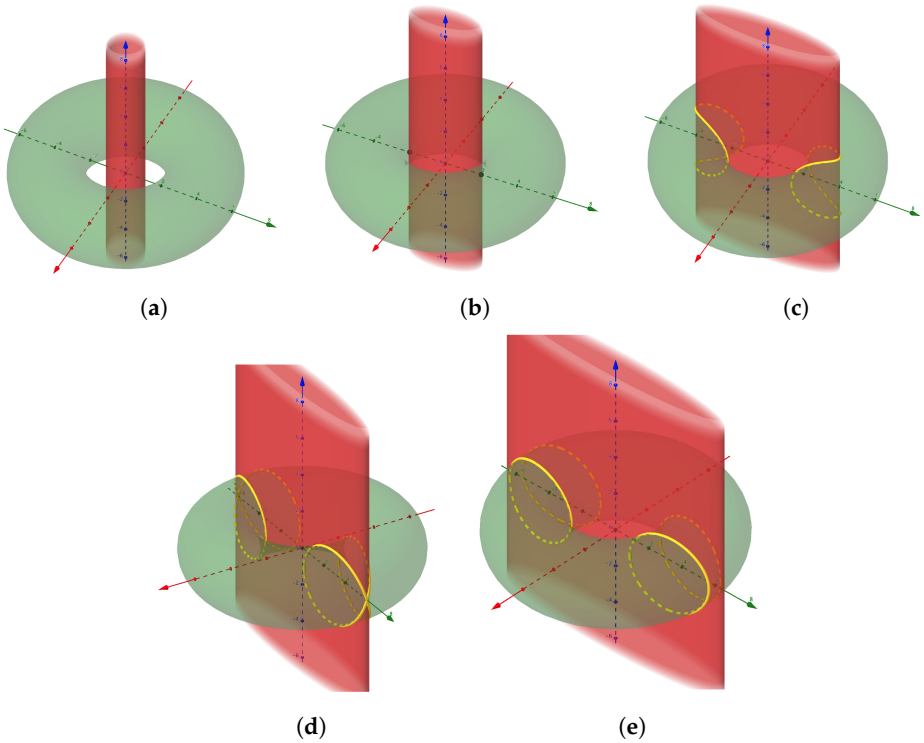


Figure 2. The cases corresponding to $a < rM - rm$, according to the values of b.

4.1.2. Next, Assume That $a = rM - rm$

It is important to note that, under this assumption, the points $(\pm(rM - rm), 0, 0)$ will invariably be included in the intersection set of the two surfaces.

We consider the following cases:

- If $b < rM - rm$, the intersection set is composed of two points (Figure 3a), corresponding to the points where the inner equatorial circle of the torus tangentially touches the cylinder.
- If $b = rM - rm$, the cylinder tangentially touches the torus at the points of its inner equatorial circle, which corresponds to the intersection of the two surfaces (Figure 3b).
- If $rM - rm < b < rM + rm$, the intersection curve is connected and has two self-intersection points, specifically the points $(\pm(rM - rm), 0, 0)$ mentioned at the very beginning of our discussion (Figure 3c).
- If $b = rM + rm$, the intersection curve is connected with four self-intersection points. In addition to the previously mentioned points, which correspond to where the torus's inner equatorial circle tangentially touches the cylinder, it also includes the points $(0, \pm(rM + rm), 0)$ (Figure 3d), corresponding to the points where the torus's outer equatorial circle touches the cylinder.
- If $b > rM + rm$, the intersection curve consists of two connected components, each with one self-intersection point (Figure 3e).

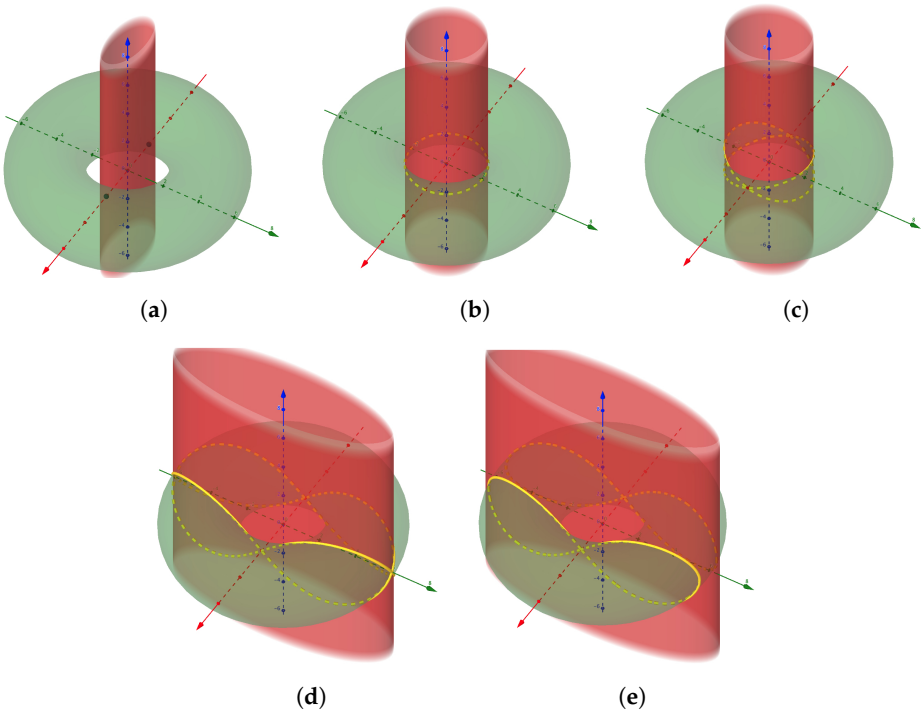
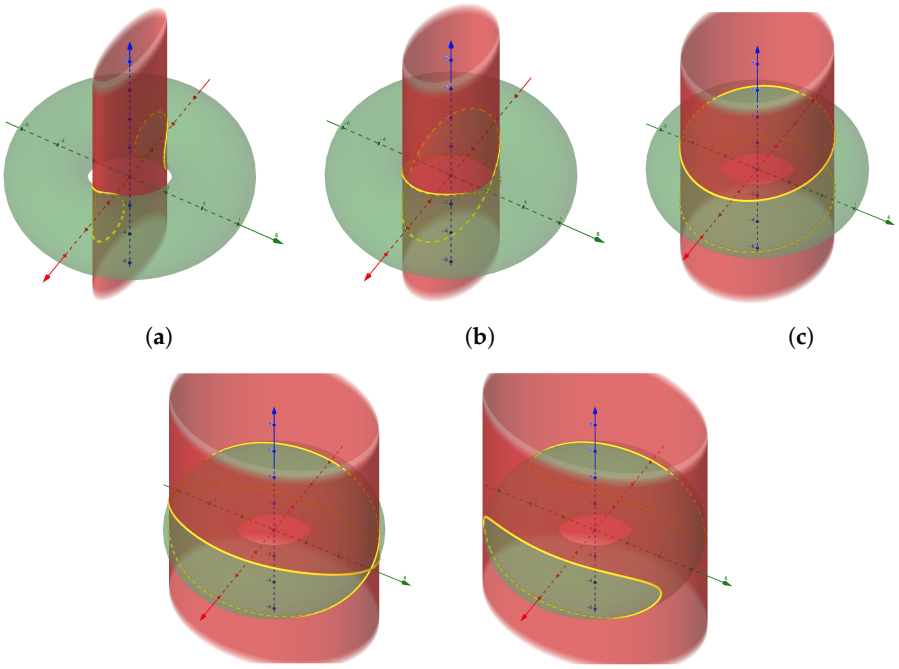


Figure 3. The cases corresponding to $a = rM - rm$, according to the values of b.

4.1.3. Now, Let Us Consider $rM - rm < a < rM + rm$

We consider the following cases:

- For $b < rM - rm$, $rM - rm < b < rM + rm$, and $b > rM + rm$, the intersection curve is composed of two connected components (Figure 4a,c,e) without self-intersection points.
- For $b = rM - rm$ or $b = rM + rm$, the intersection curve is connected with two self-intersection points at coordinates $(0, \pm(rM - rm), 0)$ and $(0, \pm(rM + rm), 0)$ (Figure 4b and Figure 4d, respectively).



(**a**) (**b**) (**c**)

(**d**) (**e**)

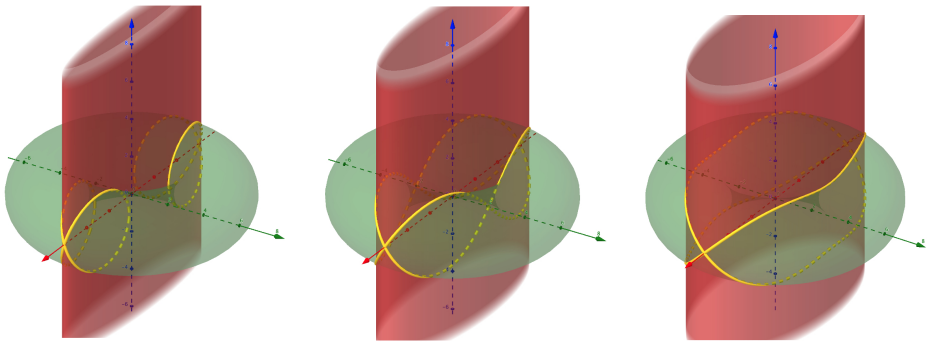
Figure 4. The cases corresponding to $rM - rm < a < rM - rm$, according to the values of b.

4.1.4. Now, Let Us Assume That $a = rM + rm$

In this case, the points $(\pm(rM + rm), 0, 0)$ will inevitably be the points of intersection of the two surfaces.

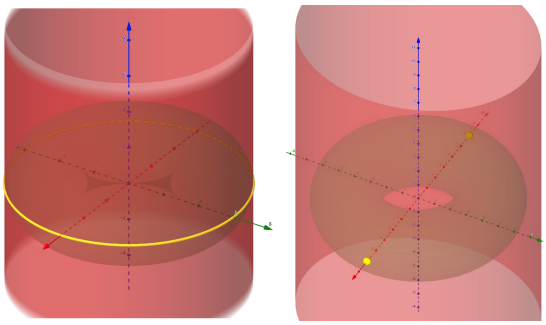
We consider the following cases:

- If $b < rM - rm$, the points $(\pm(rM + rm), 0, 0)$ are the self-intersection points of the intersection curve. This curve has two connected components (Figure 5a).
- For $b = rM - rm$, the intersection curve is a connected component with four self-intersection points at $(\pm(rM + rm), 0, 0)$ and $(0, \pm(rM - rm), 0)$ (Figure 5b).
- If $rM - rm < b < rm + rM$, the intersection curve is connected with two self-intersection points at $(\pm(rM + rm), 0, 0)$ (Figure 5c).
- If $b = rM + rm$, the cylinder tangentially touches the torus at any point of the torus's outer equatorial circle (Figure 5d).
- If $b > rM + rm$, we have a tangential intersection at the two points $(\pm(rM + rm), 0, 0)$ (Figure 5e).



(**a**) (**b**) (**c**)

Figure 5. *Cont.*



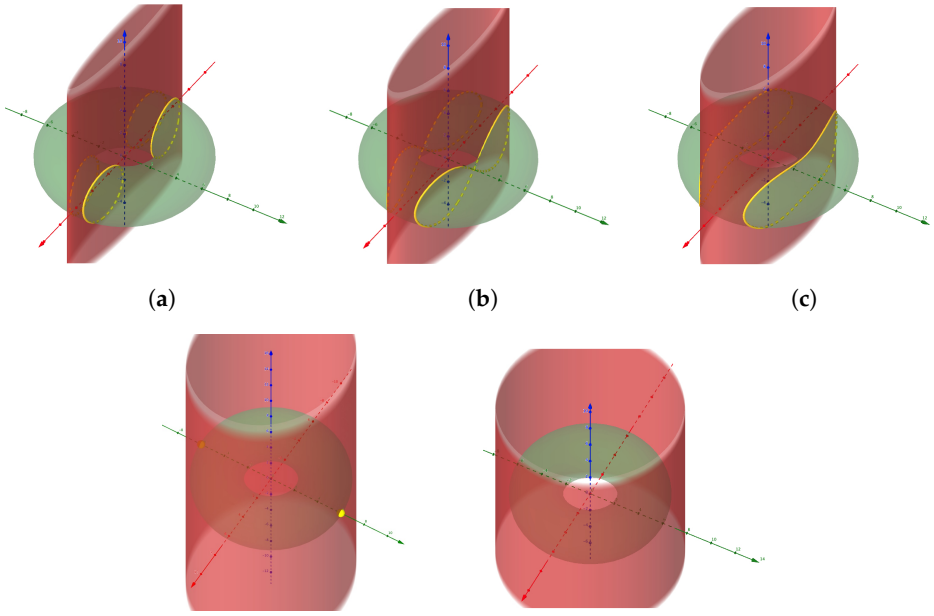
(**d**) (**e**)

Figure 5. The cases corresponding to $a = rM + rm$, according to the values of b.

4.1.5. Finally, Let Us Assume That $a > rM + rm$

We consider the following cases:

- If $b < rM - m$, the intersection curve has four connected components (Figure 6a).
- If $b = rM - rm$, the curve has only two connected components, each with a self-intersection point at $(0, \pm(rM - rm), 0)$, (Figure 6b).
- If $rM - rm < b < rM + rm$, the intersection curve only has two connected components and no self-intersection points (Figure 6c).
- If $b = rM + rm$, the cylinder tangentially touches the torus at the points with coordinates $(0, \pm(rM + rm), 0)$ (Figure 6d).
- If $b > rM + rm$, the torus is inside the cylinder, and so no common points exist between the two surfaces (Figure 6e). The intersection set is the empty set.



(**a**) (**b**) (**c**)

(**d**) (**e**)

Figure 6. The cases corresponding to $a > rM + rm$, according to the values of b.

4.2. The Case $\mathcal{T} \cap (\mathcal{E}_{b,c})_{b,c \in \mathbb{R}^+}$

This section provides the geometric and topological perspective of the intersection curve, $\mathcal{T} \cap \mathcal{E}_{b,c}$, for all admissible values of the parameters b and c, applying the procedure described in Section 3. As in the previous case, the focus is on the number of connected components and self-intersection points of these curves.

Table 2 presents the possible configurations for the intersection curve for the case under study, considering the variations and conditions imposed on the parameters $\boldsymbol{a}$ and $\boldsymbol{b}$. Next, we provide a detailed analysis of each of them.

Table 2. Case $\mathcal{T} \cap \mathcal{E}_{(b,c)}$: connected components (c.c.); self-intersection points (a.p.).

	$b < rM - rm$	$b = rM - rm$	$rM - rm < b < rm + rM$	$b = rm + rM$	$b > rm + rM$
$c < rm$	4 c.c. (Figure 7a)	3 c.c. 2 a.p. (Figure 7b)	4 c.c. (Figure 7c)	3 c.c. 2 a.p. (Figure 7d)	4 c.c. (Figure 7e)
$c = rm$	2 c.c. 4 a.p. (Figure 8a)	1 c.c. 6 a.p. (Figure 8b)	1 c.c. 4 a.p. (Figure 8c)	1 c.c. 6 a.p. (Figure 8d)	2 c.c. 4 a.p. (Figure 8e)
$c > rm$	4 c.c. (Figure 9a)	2 c.c. 2 a.p. (Figure 9b)	2 c.c. (Figure 9c)	2 points (Figure 9d) / 2 c.c. 2 a.p. (Figure 9f)	empty (Figure 9e) / 4 c.c. (Figure 9g)

4.2.1. First, Assume That $c < rm$

We consider the following cases:

- If $b < rM - rm$, $rM - rm < b < rM + rm$, and $b > rM + rm$, the intersection curve is composed of four connected components, as illustrated in Figure 7a, Figure 7c, and Figure 7e, respectively.
- If $b = rM - rm$ and $b = rM + rm$, the intersection curve has three connected components and two self-intersection points at $(0, \pm(rM - rm), 0)$ and $(0, \pm(rM + rm), 0)$ located in the same connected component (Figure 7b) and (Figure 7d), respectively.

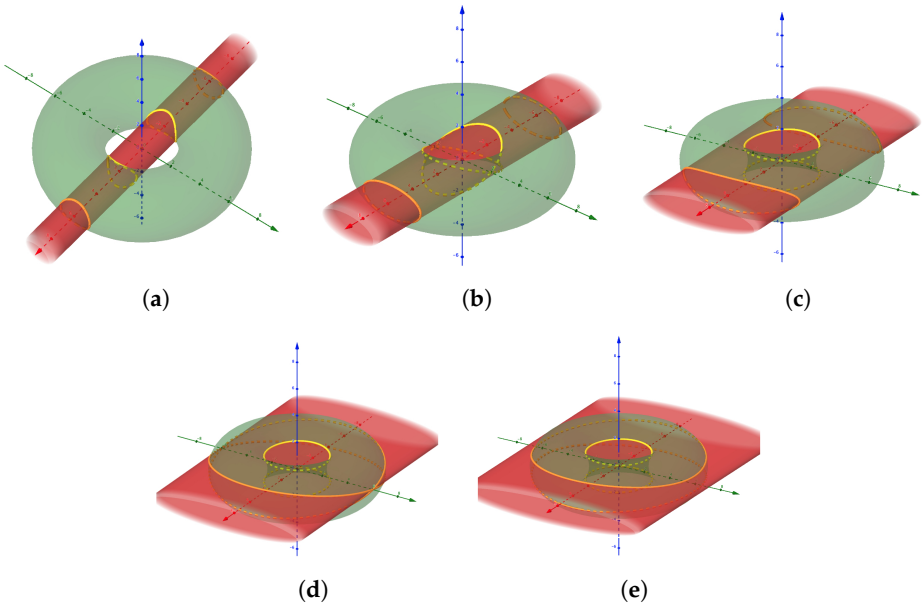
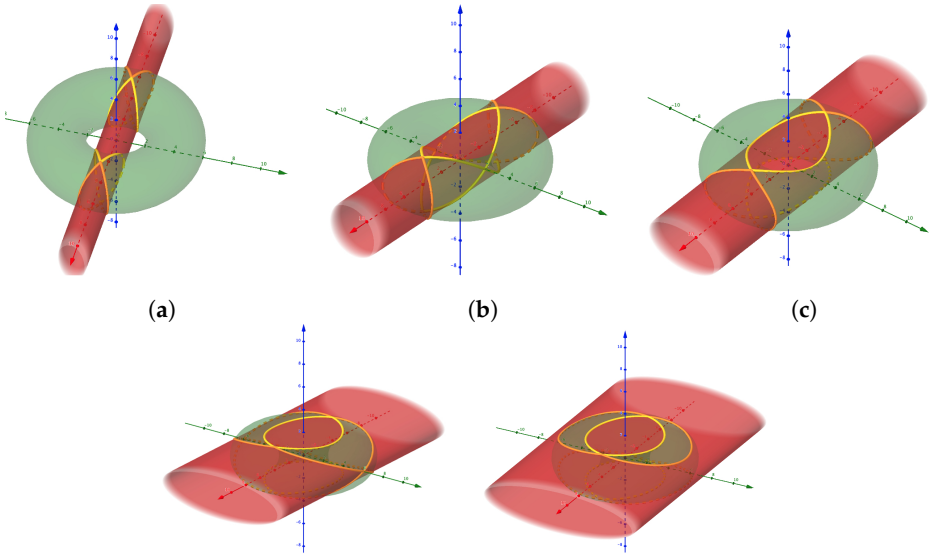


Figure 7. The cases corresponding to $c < rm$, according to the values of b.

4.2.2. Now, Assume That $c = rm$

We consider the following cases:

- For $b < rM - rm$ and $b > rM + rm$, the intersection curve has two connected components, each with two self-intersection points (Figures 8a and 8e, respectively).
- For $rM - rm < b < rM + rm$, the intersection curve is a connected component with four self-intersection points (Figure 8c).
- For $b = rM - rm$ (Figure 8b) and $b = rM + rm$ (Figure 8d), the intersection curve has six self-intersection points, including the points $(0, \pm(rM - rm), 0)$ and $(0, \pm(rM + rm), 0)$.



(**a**) (**b**) (**c**)

(**d**) (**e**)

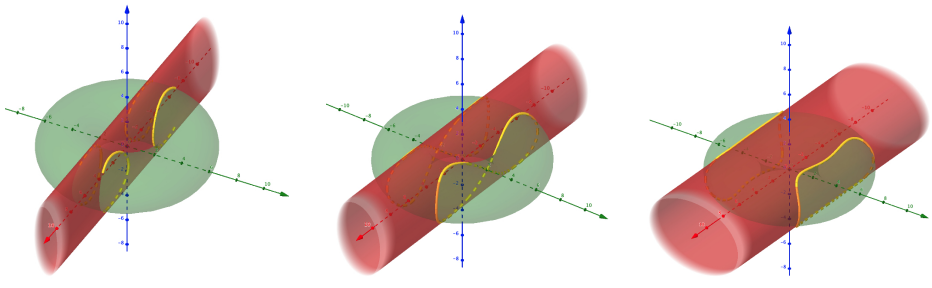
Figure 8. The cases corresponding to $c = rm$, according to the values of b.

4.2.3. Finally, Let Us Consider $c > rm$

We consider the following cases:

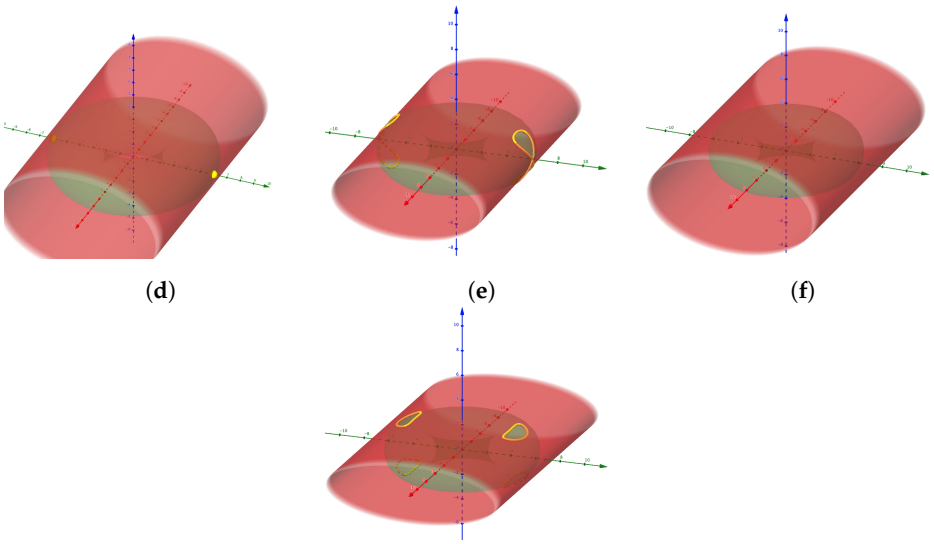
- For $b < rM - rm$ (Figure 9a), the intersection curve has four connected components and no self-intersection points.
- For $rM - rm < b < rM + rm$ (Figure 9c), the intersection curve has two connected components and no self-intersection points.
- For $b = rM - rm$, the curve is also formed by two connected components, with two self-intersection points at $(0, \pm(rM - rm), 0)$, one in each component (Figure 9b).
- For $b = rM + rm$, the points $(0, \pm(rM + rm), 0)$ are on the intersection curve. However, two situations may occur: either the intersection is formed exclusively by these two points (Figure 9d) or by two connected components, with the mentioned points being self-intersection points (Figure 9e).

Regarding the case where $b > rM + rm$, two situations may occur: either the torus is inside the cylinder (Figure 9f) or the intersection curve is formed by four connected components (Figure 9g).



(**a**) (**b**) (**c**)

Figure 9. *Cont.*



(**d**) (**e**) (**f**) (**g**)

Figure 9. The cases corresponding to $c > rm$, according to the values of b.

5. The Case $\mathcal{T} \cap (\mathcal{P}_{a,b})_{a,b \in \mathbb{R}^+}$

The methodology used for the geometric representation, algebraic description, and topological properties of the intersection curve of the torus $\mathcal{T}$ with parabolic cylinders whose generatrices are parallel to the axis of $\mathcal{T}$ is once again based on the algorithm described in Section 3.

For each $a, b \in \mathbb{R}^+$, the resultant of the two surface polynomial equations in terms of z is a parabola lying in the xOy-plane, defined by

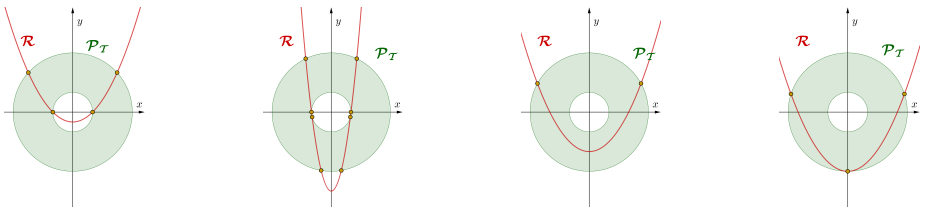
$$\mathcal{R}_{(a,b)} : a^2 b + a^2 y - b x^2 = 0. \tag{5}$$

So, the admissible region $\mathcal{A}$, the region bounded by the projection of the two surfaces onto the xOy-plane, is the intersection between the circular crown

$$\mathcal{P}_{\mathcal{T}} : (rM - rm)^2 \leq x^2 + y^2 \leq (rM + rm)^2,$$

and the parabola defined in (5).

$\mathcal{A}$ contains the cutcurve (part of the curve $\mathcal{R}_{(a,b)}$ in $\mathcal{A}$), which contains the projection in the xOy-plane of the intersection curve, $\mathcal{C}_{(a,b)}$, of the two surfaces. In Figure 10, particular cases of the admissible region $\mathcal{A}$ are presented, considering the torus $\mathcal{T}_{(O,4,2)}$ and the corresponding values of a and b mentioned there.



(**a**) $(a, b) = (2, 1)$ (**b**) $(a, b) = (2, 8)$ (**c**) $(a, b) = (4, 4)$ (**d**) $(a, b) = (5, 6)$

Figure 10. $\mathcal{A}$ considering $\mathcal{T}_{(O,4,2)}$ and $\mathcal{PC}_{(a,b)}$ for various values of a and b.

The information needed to topologically classify $\mathcal{C}_{(a,b)}$ depends on the *nature* and number of intersection points between the boundary of the circular crown and the parabola defined by Equation (5). We can compute the branches of the cutcurve using closed formulas involving radicals, and obtain, from there, the intersection curve of the two considered surfaces by lifting the branches of the cutcurve using the parametric equations of the torus (see [13]).

Analyzing the two equation systems $x^2+y^2=(rM-rm)^2 \wedge a^2b+a^2y-bx^2=0$ and $x^2+y^2=(rM+rm)^2 \wedge a^2b+a^2y-bx^2=0$, the solutions are given, respectively, by $x=a\epsilon_1 \wedge y=b({\epsilon_1}^2-1)$ and $x=a\epsilon_2 \wedge y=b({\epsilon_2}^2-1)$, where ϵ_1 is given by

$$\pm\frac{\sqrt{2}\sqrt{-a^2+2b^2\pm\sqrt{a^4-4a^2b^2+4b^2(rM-rm)^2}}}{2b},$$

and ϵ_2 is given by

$$\pm\frac{\sqrt{2}\sqrt{-a^2+2b^2\pm\sqrt{a^4-4a^2b^2+4b^2(rM+rm)^2}}}{2b},$$

note that ϵ_1 and ϵ_2 are the roots of the polynomials

$$b^2X^4+(a^2-2b^2)X^2+b^2-(rM-rm)^2 \tag{6}$$

and

$$b^2X^4+(a^2-2b^2)X^2+b^2-(rM+rm)^2\,, \tag{7}$$

respectively.

The discussion of the number of solutions depends on the analysis of the discriminant

$$\Delta_\pm := 16(b^2-(rM\pm rm)^2)b^2(a^4-4a^2b^2+4b^2(rM\pm rm)^2)^2. \tag{8}$$

It is crucial to keep in mind that the solutions to the two systems are not independent; rather, they are inherently interdependent and closely tied to the variations of the parameters a and b.

For our discussion, we also need to consider the two boundary conditions

$$t_i : b=\frac{a^2}{2\sqrt{-(rM-rm)^2+a^2}},\quad a\in]rM-rm,\sqrt{2}(rM-rm)]. \tag{9}$$

and

$$t_e : b=\frac{a^2}{2\sqrt{-(rM+rm)^2+a^2}},\quad a\in]rM+rm,\sqrt{2}(rM+rm)]. \tag{10}$$

Conditions (9) and (10) give us the cases where the resultant is tangent, respectively, to the inner and the outer circle of $\mathcal{P}_\mathcal{T}$.

Following the strategy described in Sections 4.1 and 4.2, we can sketch a diagram representing the topological behavior of $\mathcal{C}_{(a,b)}$ according to the parameters a and b, as illustrated in Figure 11.

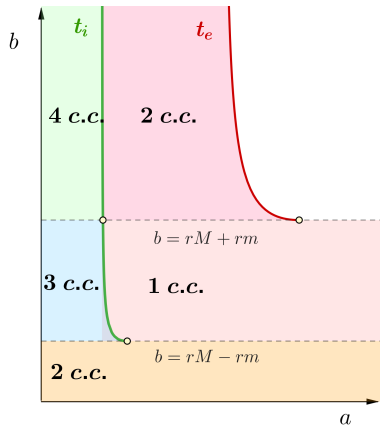


Figure 11. Map of parameters regarding the number of $\mathcal{C}_{(a,b)}$ connected components.

Let us now analyze the cases where (a, b) belongs to the graphs of t_i or t_e.

For points in the admissible region belonging to the graph of t_i, it can be algebraically verified that the silhouette curves always intersect at four points, two of which are self-intersection points of the intersection curve, except for the values $b = rM + rm$ and $a = \sqrt{2}(rM + rm)$. In the latter case, the intersection of the curves of the silhouette corresponds to three points: two on the outer curve and one on the inner curve of the silhouette curve of $\mathcal{T}$. This happens since a root of the quartic equation in the variable y (see line 7 of the symbolic algebraic computations illustrated in Figure 12a), $y = -rM + rm$, has multiplicity 2, defining the self-intersection point $(0, -rM + rm, 0)$ of the intersection curve, in addition to the points

$$(\pm\sqrt{\sqrt{rM\,rm}\,(rM - rm)}, -rM + rm + 2\sqrt{rM\,rm}, 0).$$

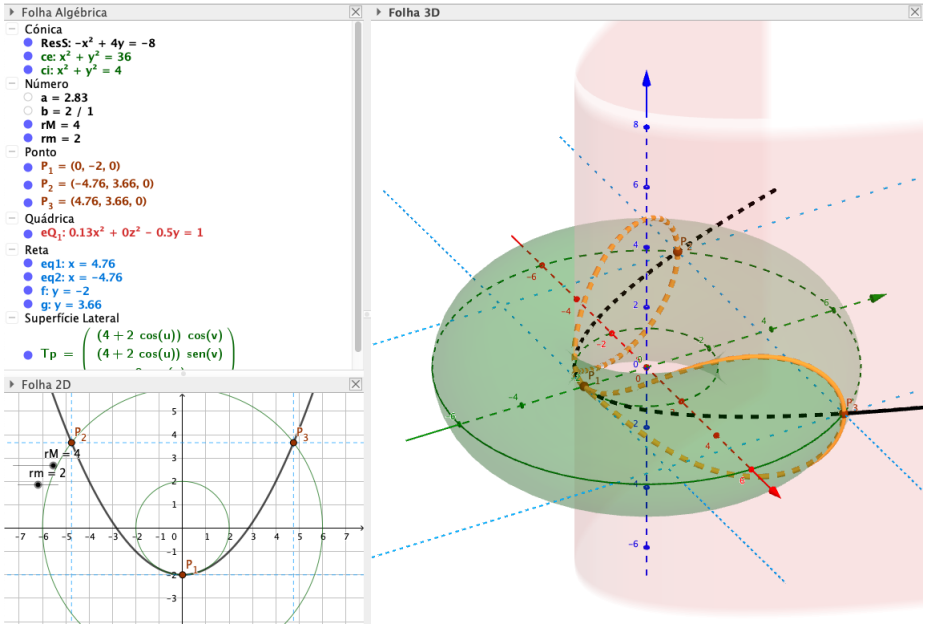
Note also that one of the solutions of the quartic equation in the variable y, $-rM + rm - 2\sqrt{rM\,rm}$, has complex solutions in the variable x (see lines 10 and 11 of Figure 12a) and should not be considered for the intersection curve of the surfaces in $\mathbb{R}^3$. This situation is also observed using GeoGebra's computational and graphic functionalities (see Figure 12b), following a specific process of parametrization [13].

For the limit curve t_e, it can be verified algebraically, considering only solutions in $\mathbb{R}$, that the silhouette curves always intersect at two points, which, after the lifting to the torus, correspond to two connected components of the intersection curve with coordinates $(\pm\sqrt{-a^2 + 2\,(rM + rm)^2}, -\sqrt{(a + rM + rm)(a - rM - rm)}, 0)$, except for the parameter values $b = rM + rm$ and $a = \sqrt{2}(rM + rm)$. In this case, the silhouette curves intersect at only one point: the point $(0, -rM - rm)$, which corresponds, after lifting, to a connected component defined by the point $(0, -rM - rm, 0)$. It should be noted that if $b = rM + rm$ and $a = rM + rm$, the $\mathcal{P}$ degenerates into two parallel planes tangent to $\mathcal{T}$ at $(\pm(rM + rm), 0, 0)$. In fact, along the limit curve t_e, the resultant remains tangent to the outer curve of the silhouette curve of $\mathcal{T}$. By performing the algebraic computations in Maple, we can obtain the graphical representations in the GeoGebra application (Figure 13).

```
> Restart
                                   Restart
> pT := (x^2 + y^2 - (rM-rm)^2) * (x^2 + y^2 - (rM + rm)^2);
                        pT := (x^2 + y^2 - (rM - rm)^2) (x^2 + y^2 - (rM + rm)^2)
> collect(pT, {x, y})
        x^4 + (2 y^2 - (rM - rm)^2 - (rM + rm)^2) x^2 + y^4 + (-(rM - rm)^2 - (rM + rm)^2) y^2 + (rM - rm)^2 (rM + rm)^2
> pP := x^2/a^2 - y/b - 1;
                                  pP := x^2/a^2 - y/b - 1
> pPs := subs(b = rM - rm, a = sqrt(2) * (rM - rm), pP)
                              pPs := x^2/(2 (rM - rm)^2) - y/(rM - rm) - 1
> solve(pPs, x^2)
Warning, solving for expressions other than names or functions is not recommended.
                                  2 (y + rM - rm) (rM - rm)
> Q1 := collect(subs(x^2 = solve(pPs, x^2), pT), y);
Warning, solving for expressions other than names or functions is not recommended.
Q1 := y^4 + (4 rM - 4 rm) y^3 + (3 (rM - rm)^2 + (2 rM - 2 rm)^2 - (rM + rm)^2) y^2 + ((rM - rm)^2 (2 rM - 2 rm) + (2 rM - 2 rm) (2 (rM - rm)^2
    - (rM + rm)^2)) y + (rM - rm)^2 (2 (rM - rm)^2 - (rM + rm)^2)
> solve(Q1, y)[1], solve(Q1, y)[2], solve(Q1, y)[3], solve(Q1, y)[4]
                  -rM + rm + 2 sqrt(rM rm), -rM + rm - 2 sqrt(rM rm), -rM + rm, -rM + rm
> solve(subs(y = solve(Q1, y)[1], pPs), x)
                  2 sqrt(sqrt(rM rm) rM - sqrt(rM rm) rm), -2 sqrt(sqrt(rM rm) rM - sqrt(rM rm) rm)
> solve(subs(y = solve(Q1, y)[2], pPs), x)
                  2 sqrt(-sqrt(rM rm) rM + sqrt(rM rm) rm), -2 sqrt(-sqrt(rM rm) rM + sqrt(rM rm) rm)
> factor(solve(subs(y = solve(Q1, y)[2], pPs), x)[1])
                                  2 sqrt(-sqrt(rM rm) (rM - rm))
> solve(subs(y = solve(Q1, y)[3], pPs), x)
                                          0, 0
> solve(subs(y = solve(Q1, y)[4], pPs), x)
                                          0, 0
```

(**a**) Maple computations

Figure 12. *Cont.*



(**b**) GeoGebra application, with $rM = 4$ and $rM = 2$.

Figure 12. Algebraic computations and graphical output for $(a, b) \in t_i$.

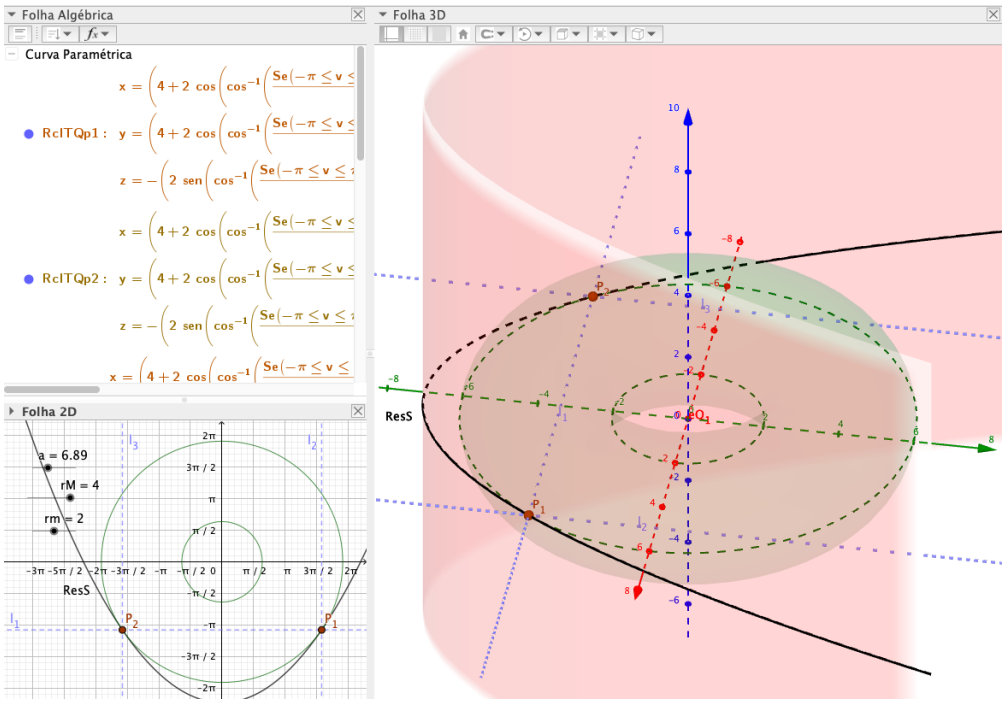


Figure 13. GeoGebra application, with $rM = 4$ and $rM = 2$.

In summary, first, let us assume that (a, b) is a point on the t_i graph. In this case, one has the following:

- ▷ If $a \neq \sqrt{2}(rM - rm)$, then $\mathcal{C}_{(a,b)}$ has three connected components (*c.c.*);
- ▷ If $a = \sqrt{2}(rM - rm)$, then $\mathcal{C}_{(a,b)}$ has three *c.c.*, one of which is the point $(0, rM + rm, 0)$;
- ▷ If $a = \sqrt{2(rM + rm)^2 - 4\sqrt{rMrm(rM + rm)^2}}$, then $\mathcal{C}_{(a,b)}$ has one *c.c.*, and $(0, rM - rm, 0)$ is a self-intersection point of the intersection curve.

Observe that $\lim_{a\to\ (rM-rm)^-} t_i(a) = +\infty$, which corresponds to a degeneration of $\mathcal{PC}_{(a,b)}$ into the union of two parallel planes tangent to the inner equatorial circle of $\mathcal{T}_{(O,rM,rm)}$. Here, $\mathcal{C}_{(a,b)}$ tends to two Bernoulli lemniscates.

Now, let us assume that (a, b) is a point on the graph of t_e.

In this case, one has the following:

- If $a \neq \sqrt{2}(rM + rm)$, then $\mathcal{C}_{(a,b)}$ has two connected components (two *c.c.*), and the two points $\mathcal{P}_{(a,b)}$ are tangent to $\mathcal{T}_{(O,rM,rm)}$;
- If $a = \sqrt{2}(rM + rm)$, then $\mathcal{C}_{(a,b)} = (\sqrt{2}(rM + rm), rM + rm)$, with one *c.c.*

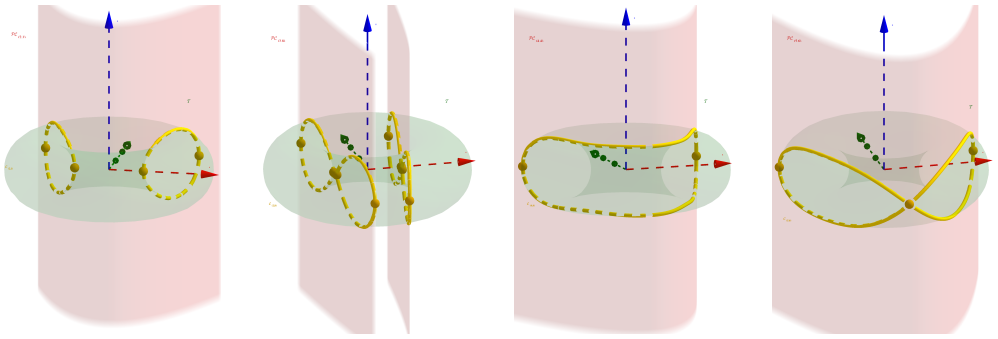
We also note that $\lim_{a\to\ (rM+rm)^-} t_e(a) = +\infty$. In this case, $\mathcal{C}_{(a,b)}$ tends to the set $\{(-(rM + rm), 0, 0), (rM + rm, 0, 0)\}$, which geometrically corresponds to a degeneration of $\mathcal{P}$ into the union of two parallel planes.

Let $b = rM - rm$ be the intersection curve containing the point $P_1(0, -(rM - rm), 0)$. In this case, one has the following:

- If $a < \sqrt{2}(rM - rm)$, then P_1 is one of three *c.c.* of $\mathcal{C}_{(a,b)}$;
- If $a \geq \sqrt{2}(rM - rm)$, then P_1 is a self-intersection point $(a.i.)$ of a curve with one *c.c.* (see Figure 14d);
- If $a \to 0^+$, then $\mathcal{C}_{(a,b)}$ approaches a curve with three *c.c.* the union of P_1 with a circle of radius $\frac{rM-rm}{2}$. Note that $\mathcal{PC}_{(a,b)}$ tends to a semi-plane.

Assuming that $b = rM + rm$, the intersection curve contains the point $P_2(0, -(rM + rm), 0)$. In this case, one has the following:

- If $a < \sqrt{2}(rM + rm)$, then $\mathcal{C}_{(a,b)}$ has two *c.c.*, and P_2 is an intersection point;
- If
$$a = \sqrt{2(rM + rm)^2 - 4\sqrt{rMrm(rM + rm)^2}}$$
then $\mathcal{C}_{(a,b)}$ has one *c.c.* and three self-intersection points, namely P_2, $(rM - rm, 0, 0)$, and $(-(rM - rm), 0, 0)$;
- If $a \geq \sqrt{2}(rM + rm)$, then $\mathcal{C}_{(a,b)}$ has one *c.c.*, reduced to a singular point, P_2;
- If $a \to 0^+$, then $\mathcal{C}_{(a,b)}$ approaches a curve with two *c.c.*, the union of two circles of radius $\frac{rM-rm}{2}$ (the intersection of $\mathcal{T}_{(O,rM,rm)}$ with the yOz-plane).



(a) $\mathcal{C}_{(2,1)}$ **(b)** $\mathcal{C}_{(2,8)}$ **(c)** $\mathcal{C}_{(4,4)}$ **(d)** $\mathcal{C}_{(5,6)}$

Figure 14. Several examples of $\mathcal{C}_{(a,b)}$.

Taking into account the study presented here, which corresponds to the variations and interdependence of the parameters a and b within the limits of the map defined in Figure 10, the complete topological classification of $\mathcal{C}_{(a,b)}$ is presented in Table 3, with respect to the number of connected components.

Table 3. Number of connected components and self-intersection points of $\mathcal{C}_{(a,b)}$.

	$0 < a < t_i(a)$	$a = t_i(a)$	$t_i(a) < a < t_e(a)$	$a = t_e(a)$
$0 < b < rM - rm$	2 *c.c.*			
$b = rM - rm$	2 *c.c.* $\{(0, -(rM - rm), 0)\}$ is one of the *c.c.*	1 *c.c.* 1 *s.p.* is $\{(0, -(rM - rm), 0)\}$	1 *c.c.* 1 *s.p.*	
$rM - rm < b < rM + rm$	3 *c.c.*	1 *c.c.* 2 *s.p.*	1 *c.c.*	
$b = rM + rm$	3 *c.c.* 1 *s.p.*	1 *c.c.* 3 *s.p.*	2 *c.c.* 1 *s.p.*	1 *c.c.* $\mathcal{P}_{(a,b)} = \{(0, -(rM + rm), 0)\}$
$b > rM + rm$	4 *c.c.*	2 *c.c.* 2 *s.p.*	2 *c.c.*	2 *c.c.* A set of two points

In Figure 15, we show the evolution of the shapes of $\mathcal{C}_{(a,b)}$, considering $\mathcal{T}_{(O,4,2)}$.

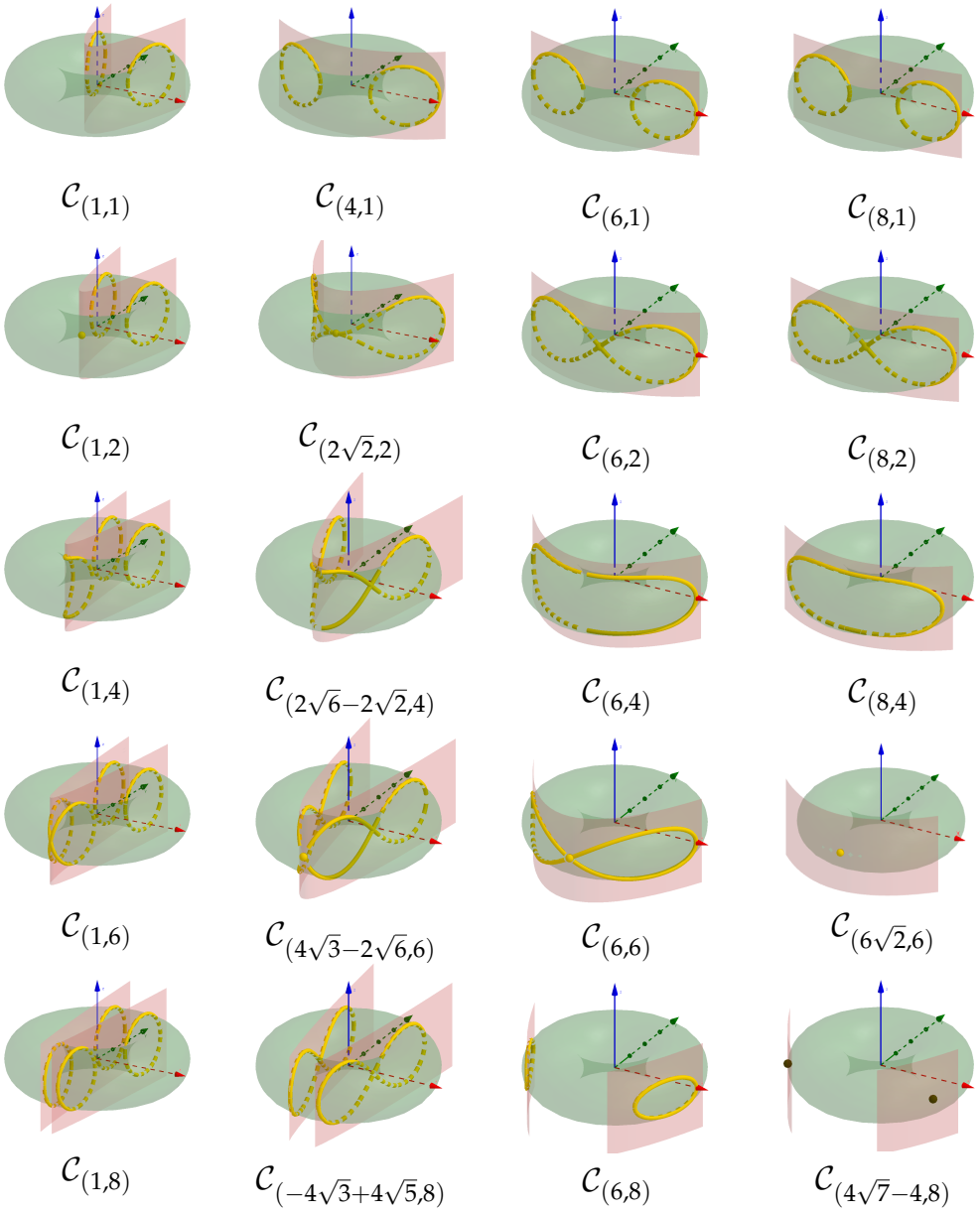


Figure 15. The intersection curve $\mathcal{C}_{(a,b)}$, considering the surfaces $\mathcal{P}$ and $\mathcal{T}_{(O,4,2)}$.

6. Conclusions

In this study, we present a method for topologically classifying the intersection curve between a torus and specific families of elliptical and parabolic cylinders. The employed

methodology makes use of an algorithm that analyzes the projection of the intersection curve onto a plane, examines its critical and singular points, and lifts it within a combined geometric, algebraic, and computational approach.

The employed methodology can be extended to other surfaces, opening up significant opportunities for advancing the mathematical knowledge and understanding of surface-to-surface intersections. The broad applicability of the algorithm has the potential to drive further breakthroughs in both theoretical and applied mathematics, promoting the development of new approaches to complex geometric problems.

By expanding the scope of this research to include additional surfaces, we can further clarify our understanding of complex surface interactions.

Advances in this topic have the potential to enhance precision in industrial design, improve simulation accuracy in robotics, and optimize computational processes in architectural modeling.

Algorithms that employ floating-point arithmetic to address this problem can achieve low running times but are sensitive to rounding errors, which can compromise their correctness [9]. In contrast, symbolic methods guarantee accurate results because they rely on exact arithmetic—provided the quadrics are precisely defined—but they typically exhibit significantly lower performance compared to numerical techniques. The proposed algorithm overcomes these difficulties by using exact algebraic expressions, enabling the determination of points where singularities exist on the intersection curves of the surfaces. Topologically classifying the intersection curves between toric surfaces and families of quadric surfaces requires a study that has not been generally possible and has been limited to specific families of quadrics, suggesting that it may be possible to obtain the classification in the general case.

Future work should continue to explore and characterize the intersection of the yorus with other families of quadrics.

Author Contributions: Conceptualization, A.B., A.T. and J.D.S.; Methodology, A.B., A.T. and J.D.S.; Investigation, A.B., A.T. and J.D.S. All authors have read and agreed to the published version of the manuscript.

Funding: This research was supported by the Center for Research and Development in Mathematics and Applications (CIDMA) through the Portuguese Foundation for Science and Technology (FCT—Fundação para a Ciência e a Tecnologia), references UIDB/04106/2020 (https://doi.org/10.54499/UIDB/04106/2020 (accessed on 15 October 2024) and UIDP/04106/2020 (https://doi.org/10.54499/UIDP/04106/2020 (accessed on 15 October 2024).

Data Availability Statement: Not applicable.

Conflicts of Interest: The authors declare no conflicts of interest.

References

1. Tu, C.; Wang, W.; Wang, J. Classifying the nonsingular intersection curve of two quadric surfaces. In Proceedings of the Geometric Modeling and Processing. Theory and Applications, GMP 2002, Wako, Japan, 10–12 July 2002; GMAP-02; IEEE Computer Society: Washington, DC, USA, 2002 ; pp. 23–32. [CrossRef]
2. Hanna, S.; Abel, J.; Greenberg, D. Intersection of Parametric Surfaces by Means of Look-Up Tables. *IEEE Comput. Graph. Appl.* **1983**, *3*, 39–48. [CrossRef]
3. Pironti, A.; Walker, M. Fusion, tokamaks, and plasma control: An introduction and tutorial. *IEEE Control Syst. Mag.* **2005**, *25*, 30–43. [CrossRef]
4. Kim, K.J.; Kim, M.S.; Oh, K. Torus/Sphere Intersection Based on a Configuration Space Approach. *Graph. Model. Image Process.* **1998**, *60*, 77–92. [CrossRef]
5. Kim, M.S. Intersecting surfaces of special types. In Proceedings of the Shape Modeling International '99. International Conference on Shape Modeling and Applications, Aizu-Wakamatsu, Japan, 1–4 March 1999; pp. 122–128. [CrossRef]
6. Kim, K.J. Circles in torus–torus intersections. *J. Comput. Appl. Math.* **2012**, *236*, 2387–2397. [CrossRef]
7. Liu, X.-M.; Liu, C.-Y.; Yong, J.H.; Paul, J.C. Torus/Torus Intersection. *Comput.-Aided Des. Appl.* **2011**, *8*, 465–477. [CrossRef]
8. Li, Q.; Zhang, S.Y.; Ye, X. Algebraic Algorithms for Computing Intersections between Torus and Natural Quadrics. *Comput.-Aided Des. Appl.* **2004**, *1*, 459–467. Available online: https://api.semanticscholar.org/CorpusID:121808748 (accessed on 15 October 2024). [CrossRef]

9. Gonzalez-Vega, L.; Trocado, A. Tools for analyzing the intersection curve between two quadrics through projection and lifting. *J. Comput. Appl. Math.* **2021**, *393*, 113522. [CrossRef]
10. Dupont, L.; Lazard, D.; Lazard, S.; Petitjean, S. Near-optimal parameterization of the intersection of quadrics. In Proceedings of the SCG '03, San Diego, CA, USA, 8–10 June 2003. Available online: https://api.semanticscholar.org/CorpusID:26759864 (accessed on 15 October 2024).
11. Trocado, A.; Gonzalez-Vega, L.; Dos Santos, J.M. Intersecting Two Quadrics with GeoGebra. In *Algebraic Informatics*; Ćirić, M., Droste, M., Pin, J.É., Eds.; Springer: Cham, Switzerland, 2019; pp. 237–248. [CrossRef]
12. Gonzalez-Vega, L.; Trocado, A. Using Maple to Compute the Intersection Curve of Two Quadrics: Improving the Intersectplot Command. In *Maple in Mathematics Education and Research*; Gerhard, J., Kotsireas, I., Eds.; Springer: Cham, Switzerland, 2020; pp. 92–100. [CrossRef]
13. Breda, A.M.R.D.; Trocado, A.E.B.d.S.; Dos Santos, J.M.D.S. Torus and Quadrics Intersection Using GeoGebra. In *ICGG 2020—Proceedings of the 19th International Conference on Geometry and Graphics*; Cheng, L.Y., Ed.; Springer: Cham, Switzerland, 2021; pp. 484–493. [CrossRef]

Disclaimer/Publisher's Note: The statements, opinions and data contained in all publications are solely those of the individual author(s) and contributor(s) and not of MDPI and/or the editor(s). MDPI and/or the editor(s) disclaim responsibility for any injury to people or property resulting from any ideas, methods, instructions or products referred to in the content.